

Visualization of Capsule Reentry Vehicle Heat Shield Ablation using Naphthalene PLIF

Christopher S. Combs^{1,*}, Noel T. Clemens¹, Paul M. Danehy²

1: Department of Aerospace Engineering and Engineering Mechanics, The University of Texas at Austin, Austin, TX, USA

2: Advanced Sensing and Optical Measurements Branch, NASA Langley Research Center, Hampton, VA, USA

* correspondent author: ccombs0022@gmail.com

Abstract The Orion Multi-Purpose Crew Vehicle (MPCV) will use an ablative heat shield and improved understanding of the ablation process would be beneficial for design purposes. Given that ablation is a multi-physics process involving heat and mass transfer, codes aiming to predict heat shield ablation are in need of experimental data pertaining to the turbulent transport of ablation products for validation. At The University of Texas at Austin, a technique is being developed that uses planar laser-induced fluorescence (PLIF) of a low-temperature sublimating ablator (naphthalene) to visualize the transport of ablation products in a supersonic flow. Since ablation at reentry temperatures can be difficult to recreate in a laboratory setting it is desirable to create a limited physics problem and simulate the ablation process at relatively low temperature conditions using naphthalene. A scaled Orion MPCV model with a solid naphthalene heat shield has been tested in a Mach 5 wind tunnel at various angles of attack in the current work. PLIF imaging reveals the distribution of the ablation products as they are transported into the heat-shield boundary layer and over the capsule shoulders into the separated shear layer and backshell recirculation region. Visualizations of the capsule shear layer using both naphthalene PLIF and Schlieren imaging compared favorably. High concentrations of naphthalene in the capsule separated flow region, intermittent turbulent structures on the heat shield surface, and interesting details of the capsule shear layer structure were observed using the naphthalene PLIF technique. The capsule shear layer was also shown to generally appear to be more turbulent at lower angles of attack. Furthermore, the PLIF signal increased steadily over the course of a run indicating that during a wind tunnel run the model heated up and the rate of naphthalene ablation increased. The shear layer showed increasing signs of turbulence over the course of a wind tunnel run as well, likely because of the combination of increased surface roughness and surface blowing rate. PLIF imaging also detected regions with a relatively low concentration of naphthalene in the capsule backshell recirculation region that are most likely the result of cross-flow-induced vortices on the capsule afterbody.

1. Introduction

In recent years, NASA has continued interest in the study of ablation due to the need to develop suitable thermal protection systems (TPS) for spacecraft that undergo planetary entry. Codes that attempt to predict ablation require a number of coupled submodels since ablation is a multi-physics process. Each of these submodels requires validation (Smits, 2009) and Reynolds-averaged Navier-Stokes (RANS) and large-eddy simulation (LES) codes, for example, require models of the turbulent transport of ablation products under variable compressibility and pressure gradient conditions. However, suitable scalar-velocity data under relevant conditions are very rare (Ho, 2007). High temperature ablation is a very complex process involving nonequilibrium gaseous and surface chemistry, spallation, radiation, etc., that is difficult and expensive to recreate in a laboratory environment. However, low temperature ablation creates a limited physics problem that can be used to simulate one aspect of the ablation process. Many low-temperature sublimating ablators have been previously used to study ablation including naphthalene (Charwat, 1968), camphor (Lipfert and Genovese, 1971), wax (Stock and Ginoux, 1971), CO₂ (dry ice) (Callaway et al., 2010), and water-ice (Silton and Goldstein, 2000), with camphor and CO₂ being employed most frequently. The focus of the majority of previous studies employing low-temperature sublimating ablators has been the determination of recession rates and changes in shape of cones, hemispheres, and other projectile-like models (Kohlman and Richardson, 1969). A technique has been developed at The University of Texas at Austin to enable visualization of the ablation products transport in a hypersonic flow using planar laser-induced fluorescence (PLIF) of naphthalene, a low-temperature sublimating ablator (Lochman, 2010; Combs et al., 2014).

PLIF is a well-developed non-intrusive flow diagnostic technique that provides a qualitative two-dimensional visualization of scalar concentration in a flow (Hanson et al., 1990). The technique uses a laser sheet to interrogate a slice in the flow containing the species of interest, which in this case is naphthalene vapor. This ultraviolet (UV) laser sheet excites the naphthalene molecules, resulting in fluorescence that is detected by a digital camera. Considering factors such as collisional quenching, temperature, and optical collection efficiencies—all of which can affect the fluorescence intensity—the PLIF signal can sometimes be converted into species number density and/or mole fraction. PLIF of species such as acetone (Lozano et al., 1992), NO (Danehy et al., 2006), and OH (Gamba et al., 2012) have been used to study numerous flowfields including various capsule geometries in high speed flows (Alderfer et al., 2007; Danehy et al., 2008; Danehy et al., 2009; Combs et al., 2013; Combs et al., 2014). Originally introduced as a fuel-marking technique in low-speed reacting flow experiments (Kaiser and Long, 2005), naphthalene PLIF has only recently been used to image ablation products in supersonic flows (Lochman, 2010; Combs et al., 2014).

NO PLIF has been used by NASA researchers to simulate the ablation process by transpiring NO gas through a port on the surface of a capsule model (Inman et al., 2008). The advantage of using a low-temperature sublimating ablator, however, is that the transported products are the result of mass transfer from the heat shield itself. A subscale capsule reentry vehicle model with a solid naphthalene heat shield has been tested in a Mach 5 wind tunnel in the current work, enabling the distribution of ablation products to be revealed by PLIF imaging as they are transported into the boundary layer and over the capsule shoulder. These images can help provide insight into scalar transport, flow structure, and potentially provide validation data for scalar-transport models.

2. Experimental Program

A. Experimental Facility

The facility used for these experiments was a Mach 5 blow-down wind tunnel. The cross-section of the test section of the facility was 152 mm wide by 178 mm tall. Optical access for laser transmission and imaging was provided by fused silica windows on the wind tunnel floor, ceiling, and sidewall. The wind tunnel was supplied by a 4 m³ storage tank held at approximately 15.5 MPa and the plenum pressure was maintained at approximately 2.48 MPa. The flow was electrically heated to achieve a stagnation temperature of about 360 K in order to increase the sublimation rate of the naphthalene heat shield. These conditions resulted in a Reynolds number based on model diameter (Re_D) of 1.0×10^6 .

B. Naphthalene Chemistry

Naphthalene, C₁₀H₈, (commonly known as Moth Balls?) is a polycyclic aromatic hydrocarbon (PAH) and is a byproduct of many combustion processes. A white crystalline solid at room temperature, naphthalene has a relatively low melting point at 353 K. The low melting point allows naphthalene crystals to easily be melted down and used for making molds of various shapes and sizes. The vapor pressure of naphthalene is approximately 12 Pa at 300 K, but increases by over two orders of magnitude to 1.4 kPa at 360 K (Kruif et al., 1981). A relatively large molecule, gaseous naphthalene possesses a wide and essentially continuous band of vibronic energy levels in the UV, absorbing electromagnetic radiation from the vacuum UV to approximately 310 nm (Du et al., 1998). Excitation of naphthalene with a UV light source results in broadband fluorescence between 300 and 400 nm (Du et al., 1998). This property of naphthalene makes it a candidate for PLIF imaging, as high-intensity light sources such as frequency-quadrupled Nd:YAG lasers, KrF lasers, and various dye laser configurations can be used to excite the molecule.

C. Model Geometry

The model geometry for this study consisted of a scaled Orion Multi-Purpose Crew Vehicle (MPCV) shaped model with smooth outer mold lines based on the scaled dimensions provided by Buck et al. The model consisted of an aluminum capsule backshell, a separate heat shield piece, and a wire “mesh” to give the solid naphthalene heat shield structural integrity (Fig. 1(a)). The mesh was mounted to sixteen 6-32 screws that protruded approximately 4 mm from the aluminum surface. The heads of the screws were at least 2 mm below the surface of the heat shield. Thin-gauge wire was then wrapped around the bolts, creating a mesh.

Without this mesh, the naphthalene heat shield would not adhere to the aluminum model and would not remain attached during wind tunnel runs. However, even with the mesh, naphthalene would still break apart from the model during wind tunnel startup for some tests. Data from these wind tunnel runs is not presented here, but for this technique to be successful it is important to have a relatively quick wind tunnel startup or to place a protective covering on the model until the freestream flow has been fully established. The aluminum model was scaled to have a 50 mm maximum heat shield diameter and was attached to a 12.7 mm diameter stainless steel sting. The sting was mounted to a strut that was fixed to the wind tunnel floor. Four different strut configurations were used in this experimental campaign, allowing four different angles of attack (0° , 12° , 24° , and 52°) to be tested. Schlieren imaging was conducted in a different experimental campaign than the PLIF and used a solid aluminum heat shield rather than a naphthalene one.

The process for creating the naphthalene heat shield involved placing the capsule model in a mold (Fig. 1(b)) and pouring heated liquid naphthalene through a hole in the aftbody near the apex of the model. The mold assembly (Fig. 1(c)) would then be allowed to cool at room temperature for approximately three hours to allow the naphthalene to solidify. Next, the mold would be disassembled and any excess naphthalene on the capsule backshell would be carefully removed to ensure that the naphthalene-aluminum junction was smooth. It was also verified that no air pockets were formed in the naphthalene during the molding process. At this point the model was ready for testing and was mounted in the Mach 5 wind tunnel test section. During wind tunnel shutdown, the remaining naphthalene on the model was destroyed, preventing images of the model from being captured post-run. A new heat shield was molded before each wind tunnel run and a completed model is shown in Fig. 2 below.

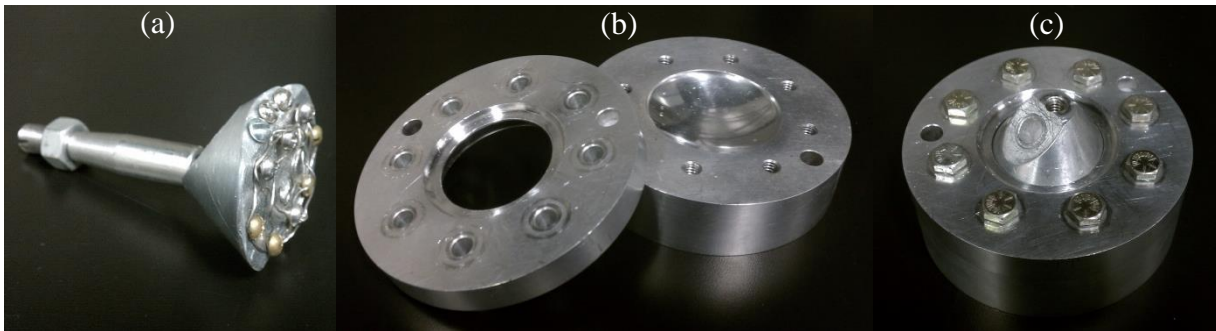


Fig. 1 (a) Orion MPCV model and sting without naphthalene heat shield, (b) top and bottom halves of mold assembly for creating naphthalene heat shield, and (c) fully-assembled mold with capsule model installed, ready for liquid naphthalene.



Fig. 2 Orion MPCV model at 52° angle of attack configuration with naphthalene heat shield installed in the Mach 5 wind tunnel facility at The University of Texas at Austin.

D. Experimental Setup

PLIF of naphthalene vapor was used to obtain a qualitative measure of the concentration of ablation products in the flow. The laser system consisted of a frequency-quadrupled Nd:YAG laser with a 266 nm output operating at a rate of 10 Hz. This wavelength was selected to excite naphthalene vapor molecules, which absorb UV radiation as discussed earlier. The laser energy was maintained at approximately 30 mJ/pulse, corresponding to an irradiance of 18 kW/mm², in order to remain below the saturation threshold of the naphthalene vapor based on previous research (Lochman, 2010). It was also confirmed that the ablation process was not significantly altered by the laser impinging on the surface of the model. The UV laser beam was oriented by a series of laser mirrors so that it passed up to the top of the wind tunnel facility where it was formed into a laser sheet using conventional sheet forming optics, as seen in Fig. 3. The resulting laser sheet was about 1 mm thick (FWHM) in the measurement region and approximately 75 mm wide. The naphthalene fluorescence was imaged onto a back-illuminated CCD camera (Apogee Alta U47), which had quantum efficiency of about 57% in the near UV and read noise of 9 e⁻ RMS. The camera was oriented normal to the laser sheet. The camera was fitted with a 100 mm focal length f/2.8 UV lens (Cerco) operated at full aperture and included a 20 mm extension ring for close focusing. A series of Schott colored glass filters (two WG-295 filters and one UG-11 filter) were placed in front of the lens to block scattered laser light and reduce the amount of solid state naphthalene fluorescence imaged by the CCD. The imaging field of view was about 50 mm x 50 mm. The images were obtained at a rate of approximately 1/3 Hz with a 30 millisecond exposure time and about 20 images were acquired per wind tunnel run. The experiment was synchronized using several Stanford Research Systems digital delay generators to ensure that images were acquired while the laser was firing.

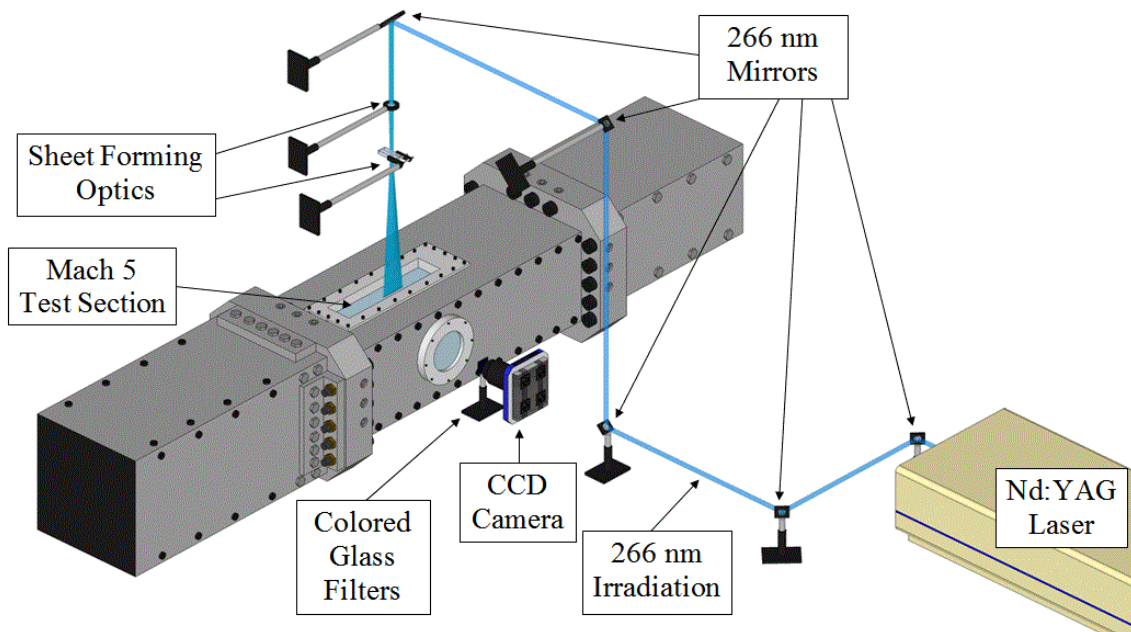


Fig. 3 Schematic of the setup used for naphthalene PLIF experiments in the Mach 5 wind tunnel facility. Flow is from bottom left to top right.

E. PLIF Flow Visualization Image Processing

Single-shot PLIF images were processed by first removing the background and then were corrected for variations in the mean intensity profile of the laser sheet. Single-shot sheet corrections were not made. The mean laser sheet spatial intensity variation was measured by imaging the fluorescence from a cell filled with acetone vapor. Approximately 20 mL of acetone was placed inside the cell and the cell was immediately closed. The liquid acetone would quickly evaporate, filling the cell with an essentially uniform distribution of acetone vapor. The cell was then placed inside the wind tunnel test section with the capsule model removed, allowing the acetone vapor to be excited with the 266 nm output from the frequency-quadrupled Nd:YAG laser. The fluorescence from the excited acetone vapor molecules was then captured with the same CCD camera used for the PLIF experiments. Since the acetone vapor was distributed uniformly in the cell,

the images of the acetone fluorescence provided a two-dimensional laser sheet intensity profile. In order to determine a mean laser-sheet intensity profile, 50 acetone fluorescence images were averaged. The single-shot images obtained during the runs were then divided by this laser-sheet intensity profile to correct for spatial variations in laser energy. No correction was made for potential laser absorption by naphthalene vapor. Additionally, in many of the subsequent figures, the PLIF intensity is presented in a logarithmic scale to improve the visibility of the entire flowfield without saturating other parts of the image.

F. Virtual Diagnostics Interface (ViDI)

The Virtual Diagnostics Interface (ViDI) (Schwartz, 2003) is a software tool developed at NASA Langley Research Center that provides unified data handling and interactive three-dimensional display of experimental data and computational predictions. It is a combination of custom-developed software applications and Autodesk® 3ds Max®, a commercially available, CAD-like software package for three-dimensional rendering and animation (Autodesk, 2006). ViDI technology can be applied to three main areas: 1) pre-test planning and optimization; 2) visualization and analysis of experimental data and/or computational predictions; and 3) establishment of a central hub to visualize, store, and retrieve experimental results. For this experiment, ViDI was used primarily for post-test visualization of the PLIF data as in Alderfer et al.

3. Experimental Results and Discussion

Naphthalene PLIF images were collected in the Mach 5 wind tunnel facility at The University of Texas at Austin's Pickle Research Campus. The first image set is shown in Fig. 4, a time-sequence of PLIF images at 0° angle of attack. The elapsed time between Fig. 4(a) and 4(f) is approximately one minute. The shear layer is clearly marked in Fig. 4 by the naphthalene PLIF technique since naphthalene vapor accumulates in the afterbody recirculation region. In Fig. 4 the shear layer appears to be laminar near the leeward shoulder of the capsule with potentially turbulent structures further downstream. In general, the shear layer appears to be most laminar near the leeward shoulder of the capsule for all images and shows signs of transition to turbulence further downstream, which is consistent with previous investigations of capsule shear layers (Combs et al., 2013). These potentially turbulent structures occur further upstream with each successive image, causing the shear layer to appear more turbulent over the course of the run. In Fig. 4(f) the shear layer looks to have undergone a complete transition to turbulence as laminar structures are not evident even at the leeward shoulder of the capsule. Another change that can be seen in the images with respect to elapsed time is that the naphthalene PLIF signal increases significantly over the course of a wind tunnel run. This increase in signal is a result of the naphthalene heat shield heating up during the run. Since the vapor pressure of naphthalene is a strong function of temperature, the sublimation rate of naphthalene increases substantially as the model heats up, leading to elevated concentrations of naphthalene vapor introduced into the flow and thus a rise in PLIF signal. Lastly, there appears to be a region of relatively low naphthalene signal located near the sting on the capsule afterbody in the separated flow region in Fig. 4. This low-signal region appears to stay in approximately the same location for all the images in the figure. Less noticeable, there is another low-signal region located farther upstream near the leeward shoulder of the capsule whose position also remains relatively fixed during the run. These structures—most likely the result of cross-flow-induced vortices—are indicated by arrows in Fig. 4e but can be seen in the other images as well.

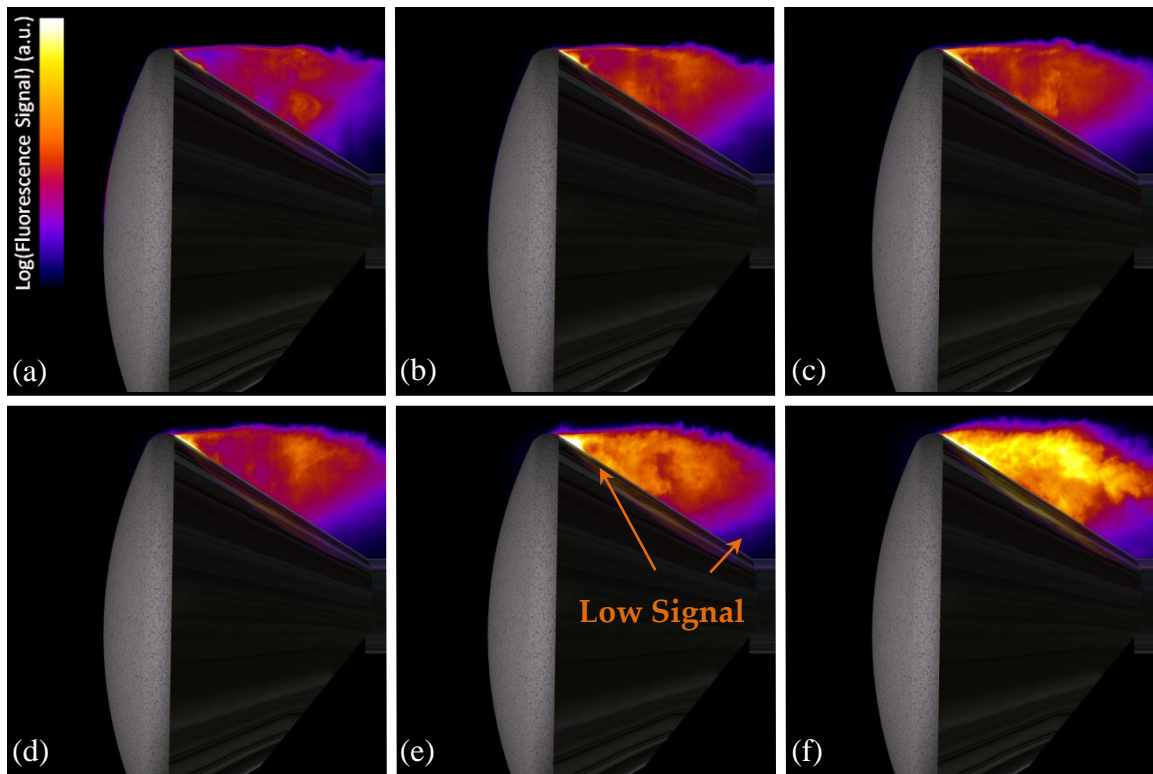


Fig. 4 Naphthalene PLIF images of a capsule model at 0° angle of attack. Images were collected during one run and images a-f are sequential in time, separated by approximately ten seconds each.

Figure 5 is also a time-sequence of PLIF images recorded during a single run but for the case of a 12° angle of attack. Once again, the elapsed time between Fig. 5(a) and 5(f) is approximately one minute. Similar to what is seen in Fig. 4, the shear layer is visualized in the images by the naphthalene vapor accumulated in the capsule afterbody recirculation region. Another similarity to Fig. 4 is the development of the shear layer during the wind tunnel run. While the shear layer appears to be laminar near the leeward shoulder of the capsule in Fig. 5(a), transition to turbulence appears to have occurred by the end of the run, depicted in Fig. 5(f). The PLIF signal can also be seen to increase with time, reemphasizing that the model is heating up over the course of the run, leading to increased naphthalene sublimation and a subsequently elevated PLIF signal. Regions of relatively low PLIF signal are also shown in the images in Fig. 5. The relatively laminar region near the sting appears to be smaller than the one seen in Fig. 4, however, in Fig. 5(f) a well-defined elliptical boundary between high and low signal can be seen, further suggesting the presence of a spanwise vortical structure on the capsule afterbody preventing naphthalene vapor from entering its core. The upstream low-signal region near the leeward shoulder of the capsule is present in Fig. 5 as well. As in Fig. 4, this feature is more subtle and has a poorly defined boundary compared to the low-signal region near the sting. There are, however, some flow structures that can be identified in the 12° case in Fig. 5 that were not visualized for the 0° case in Fig. 4. First, intermittent turbulent structures on the heat shield surface can be seen in all six images of Fig. 5 but not Fig. 4. These structures were most likely not visualized in the 0° angle of attack case due to the relatively short development length for the boundary layer on the heat shield surface, leading to a physically thinner boundary layer (perhaps still laminar) that is difficult to visualize.

Another flow feature visualized exclusively for the 12° angle of attack case is a series of elongated naphthalene vapor structures that emanate from the upper edge of the shear layer, seen most clearly in Fig. 5(d)-(f). Four zoomed-in images focusing on this feature can also be found in Fig. 6. These wispy streaks are nearly vertical in the images but are at an angle of about 45° with respect to the flow direction, with the features propagating in the opposite direction of a Mach wave or shock in a left-to-right supersonic flow. The source of these structures is not known at this time, but it is possible they are turbulent structures that originate in the upstream boundary layer and then are strained and stretched by the rapid expansion around the leeward shoulder.

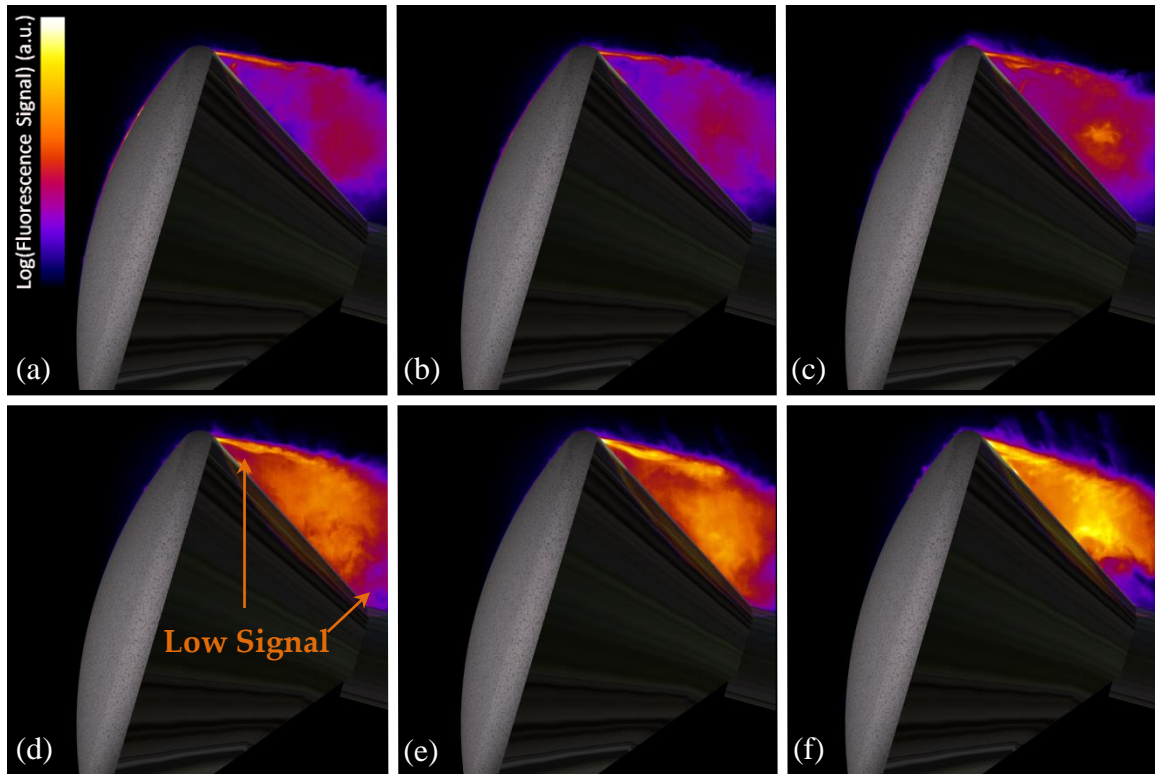


Fig. 5 Naphthalene PLIF images of a capsule model at 12° angle of attack. Images were collected during one run and images a-f are sequential in time, separated by approximately ten seconds each.

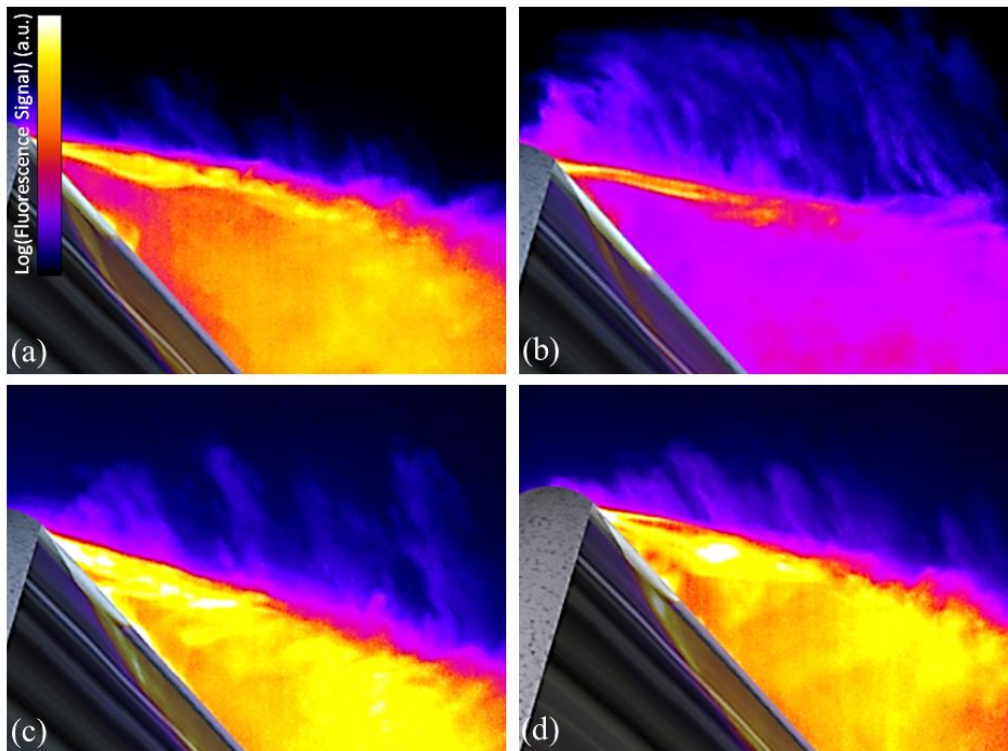


Fig. 6 Naphthalene PLIF images highlighting elongated blue-colored (low signal intensity) naphthalene structures emanating from the upper edge of the shear layer at 12° angle of attack.

A time-sequence of PLIF images for the 24° angle of attack case is presented in Fig. 7 where the elapsed time between Fig. 7(a) and 7(f) is approximately one minute. As expected based on the previous figures, the PLIF signal can be seen to increase with time due to the heating of the model. Also, as in the previous figures, the shear layer is the most clearly visualized flow structure in the image set due to the high

concentration of naphthalene in the afterbody recirculation region. However, while the shear layer appeared to transition from a laminar to a turbulent condition over the course of the 0° and 12° runs, the shear layer appears to stay effectively laminar for the majority of the images shown in Fig. 7. While a small disturbance far downstream of the leeward shoulder can begin to be seen in Fig. 7(c), this disturbance does not become amplified and propagate upstream in later images. The exact nature of the shear layer is difficult to determine in each image—particularly in Fig. 7(f)—but there are fewer instabilities visualized than in Fig. 4 or Fig. 5. Considering that the freestream Reynolds number is effectively constant over the course of the run, the onset of transition is most likely due to the change in the nature of the heat shield surface as a result of the ablation process. As the heat shield ablates, its surface becomes rough, which could lead to transition to turbulence. Additionally, the mass transfer rate or blowing rate of naphthalene vapor on the heat shield surface increases over the course of the run, which could affect turbulent transition. Given that at lower angles of attack the model appears as a larger obstruction to the flow, one would imagine that, for example, the 0° angle of attack case would undergo a more rapid change in heat shield surface than the 24° angle of attack case. This would mean that the heat shield is altered more rapidly at lower angles of attack, leading to turbulent transition in the shear layer earlier in the run. Indeed, the shear layer transitions earliest for the 0° angle of attack case and might not transition at all in the 24° angle of attack case.

Not visualized in Fig. 7 are intermittent turbulent structures on the heat shield surface. This feature was expected to be seen in this image set since turbulent structures existed on the heat shield surface for the 12° case and the 24° case has a longer development length for the heat shield boundary layer from the stagnation point. However, the image set in Fig. 7 has a lower signal-to-noise ratio than the set in Fig. 5, which could be the reason these structures are not observed. It can be seen in Fig. 7 that there is a certain amount of naphthalene vapor visualized on the heat shield surface but the signal-to-noise ratio is not high enough for individual flow structures to be resolved. Similarly, it is possible that the elongated streaks seen in Fig. 5 and Fig. 6 exist for the 24° case as well but were not visualized in the image set presented in Fig. 7 due to low signal levels. Looking closely at the images in Fig. 7, a noticeable amount of PLIF signal can be seen above the shear layer but the signal level is again not high enough for detailed structures like those seen in Fig. 6 to be identified.

In addition to the flow structures already discussed, the regions of relatively low PLIF signal are again visualized in Fig. 7. The region near the leeward shoulder is difficult to detect due to the low overall signal levels in the images but the boundary between low and high signal in the region near the sting is perhaps more crisp than in any other image set. Similar to what was seen in Fig. 5 this boundary could be broadly termed as elliptical and is reminiscent of a vortex core. Examples of these low signal regions are presented in Figs. 8 and 9, where Fig. 8 provides examples of the low-signal region near the capsule sting and select examples of low-signal regions near the leeward shoulder of the capsule can be found in Fig. 9. Again, notice how sharp the separation between high and low signal can be near the capsule sting, as seen in Fig. 8. As mentioned before, this evidence coupled with the often rounded shape of these regions indicates the structures are the result of relatively steady spanwise vortices forming in the recirculation region on the capsule backshell surface. The images in Fig. 9 corroborate this claim as the low-signal region near the leeward shoulder of the capsule is highlighted in four different examples. Most interestingly, Fig. 9(a) contains an almost perfectly circular low-signal region near the leeward shoulder of the capsule, suggesting a spanwise vortex. A highly similar structure is visualized in Fig. 9(d).

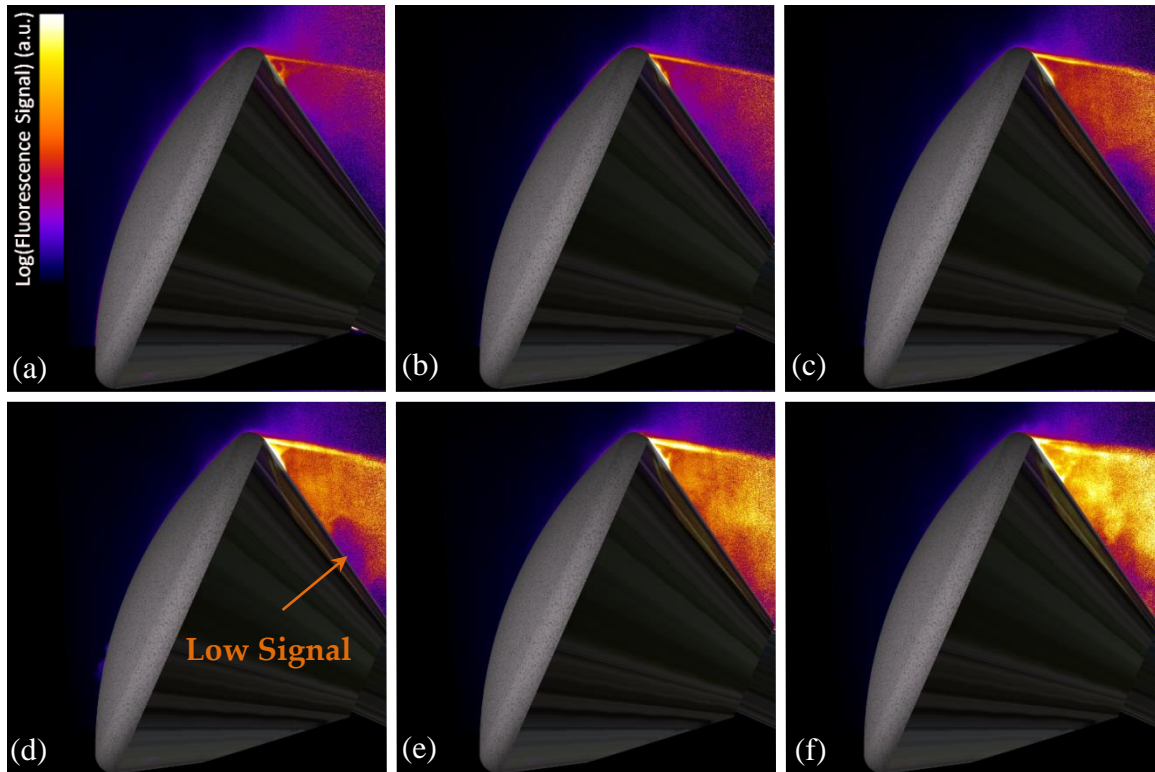


Fig. 7 Naphthalene PLIF images of a capsule model at 24° angle of attack. Images were collected during one run and images a-f are sequential in time, separated by approximately ten seconds each.

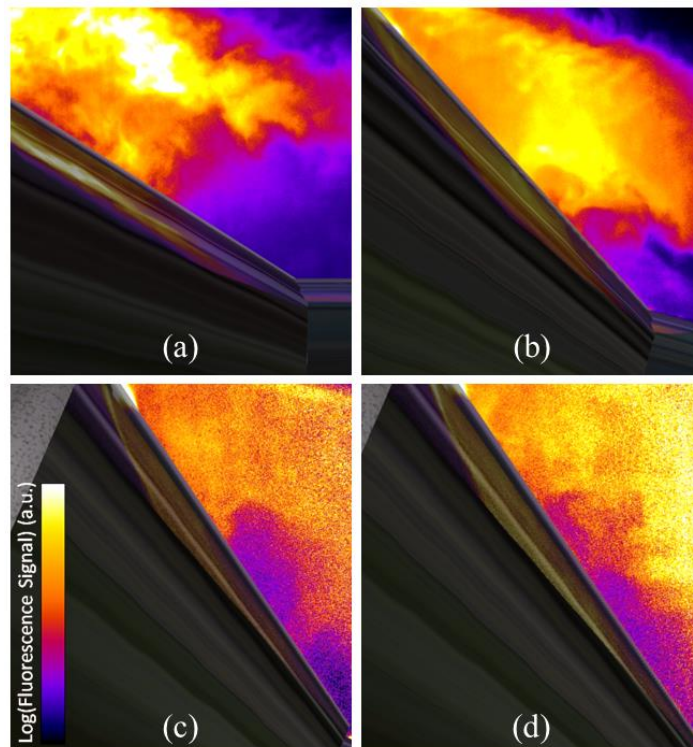


Fig. 8 Higher magnification naphthalene PLIF images highlighting low signal regions observed in the capsule recirculation zone near the model sting at (a) 0°, (b) 12°, (c) 24°, and (d) 24° angle of attack.

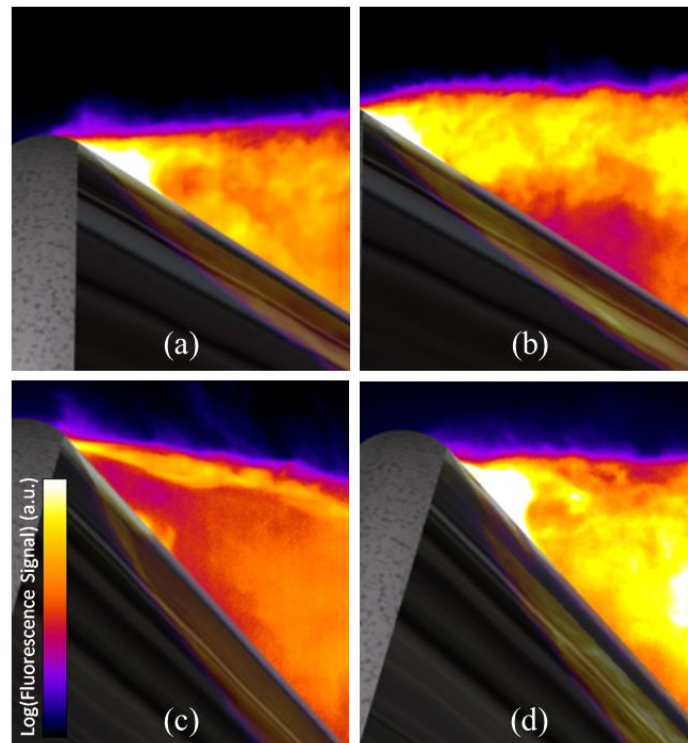


Fig. 9 Higher Magnification naphthalene PLIF images highlighting low signal regions observed in the capsule recirculation zone near the leeward shoulder at 0° angle of attack (a and b) and 12° angle of attack (c and d).

A time-sequence of PLIF images at 52° angle of attack is shown in Fig. 10. As in the previous image sequences, the elapsed time between Fig. 10(a) and 10(f) is approximately one minute. Owing to the large change in angle of attack, this image set is quite different than the ones shown for the 0° (Fig. 4), 12° (Fig. 5), and 24° (Fig. 7) angle of attack cases. Although the PLIF signal is still relatively high in the shear layer, the field of view for this image set was focused on the heat shield surface. At such a high angle of attack the surface of the heat shield occupied almost the entire field of view, preventing any determinations as to the nature of the shear layer from being made. Turbulent structures on the heat-shield surface were consistently visualized for the 52° angle of attack case and can be seen most clearly in Fig. 10(e) and 10(f). These structures appeared more frequently for the 52° angle of attack case than any other case tested because this angle of attack has the longest development length for the boundary layer (from the stagnation point which moved further upstream as the angle of attack increased) and the boundary layer seems to be the most turbulent and the thickest at the leeward shoulder (and hence the easiest to visualize). Interestingly, the presence of turbulent structures on the heat shield surface does not seem to correlate with transition of the shear layer since the shear layer was more likely to be laminar at higher angles of attack but the presence of intermittent structures on the heat shield surface is also most likely at higher angles of attack.

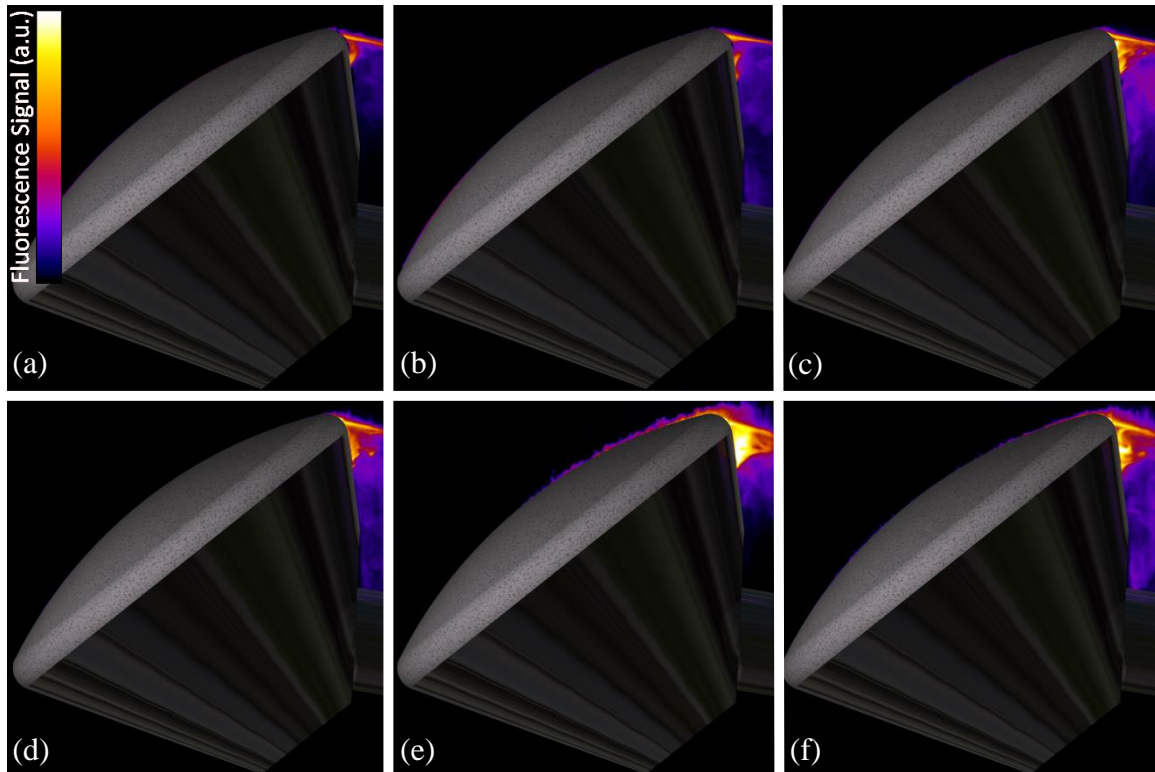


Fig. 10 Naphthalene PLIF images of a capsule model at 52° angle of attack. Images were collected during one run and images a-f are sequential in time, separated by approximately ten seconds each.

To further investigate the nature of the structures observed on the surface of the heat shield at a 52° angle of attack, additional runs were conducted with the camera field of view focused on the approximate center of the heat shield surface (Fig. 11) and on the leeward shoulder of the capsule (Fig. 12). The images in Fig. 11 were recorded sequentially in time and approximately six seconds elapsed between the acquisition of each image while approximately three seconds elapsed between the acquisition of each image in Fig. 12. Some of the same trends observed in the capsule recirculation region for the lower angle of attack cases can be found in the image sets presented in Figs. 11 and 12 when looking at the turbulent structures on the heat shield surface. First, it can be seen in both figures that the size of the structures increases with run time, with the largest structures observed in the later images. This suggests that the boundary layer on the heat shield surface is becoming more turbulent as run time increases. Again, this is most likely the result of roughening of the heat shield surface and an increased naphthalene blowing rate. The increased naphthalene sublimation rate with run time also results in an overall increase in PLIF signal intensity, as the later images (Figs. 11(e), 11(f), 12(e), and 12(f)) have higher signal levels than at the earlier times (Figs. 11(a), 11(b), 12(a), and 12(b)). Lastly, comparing Figs. 11 and 12 illustrates the growth of the turbulent boundary layer on the surface of the heat shield. As one would expect, for a similar amount of elapsed time, the structures in Fig. 12 are always larger than the ones seen in Fig. 11. For example, examining Fig. 11(a), the turbulent structures are few and exist on a relatively small scale near the center of the heat shield surface. However, further downstream in Fig. 12(a) (at approximately the same time after the beginning of the run), significantly larger structures can be seen passing over the leeward shoulder of the capsule as the turbulent boundary layer has developed along the heat shield surface.

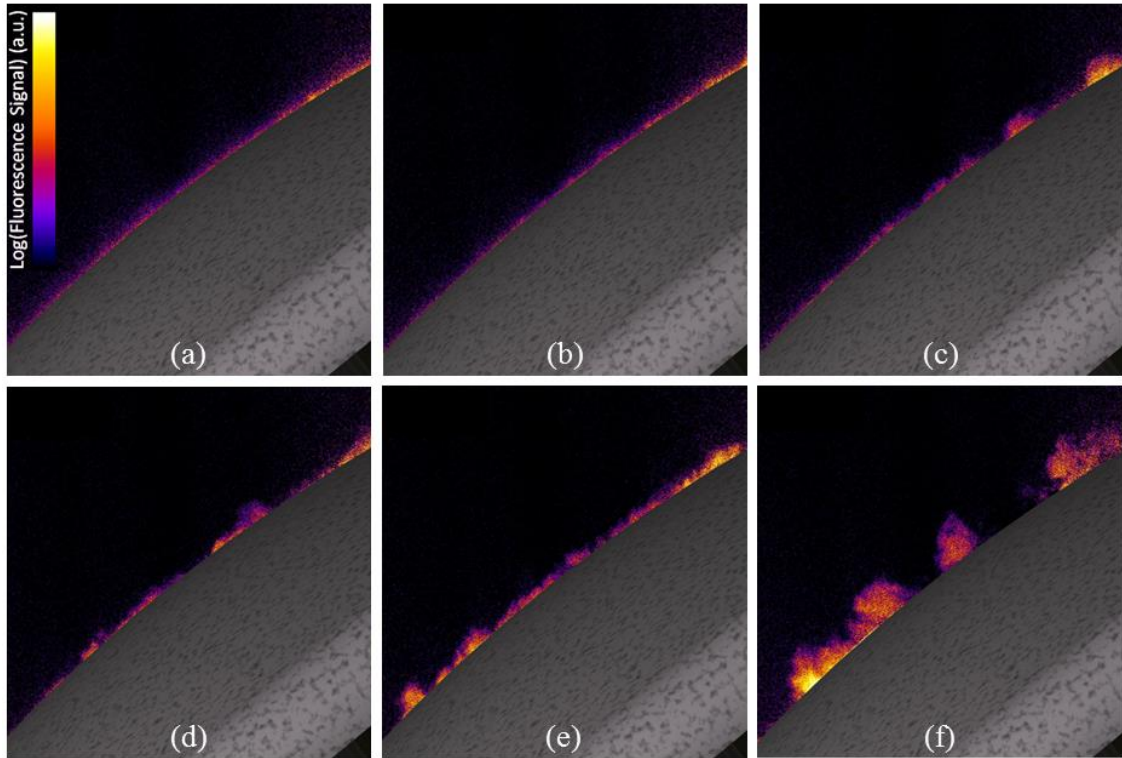


Fig. 11 Naphthalene PLIF images of a capsule model at 52° angle of attack focused on the surface of the heat shield. Images were collected during one run and images a-f are sequential in time, separated by approximately six seconds each.

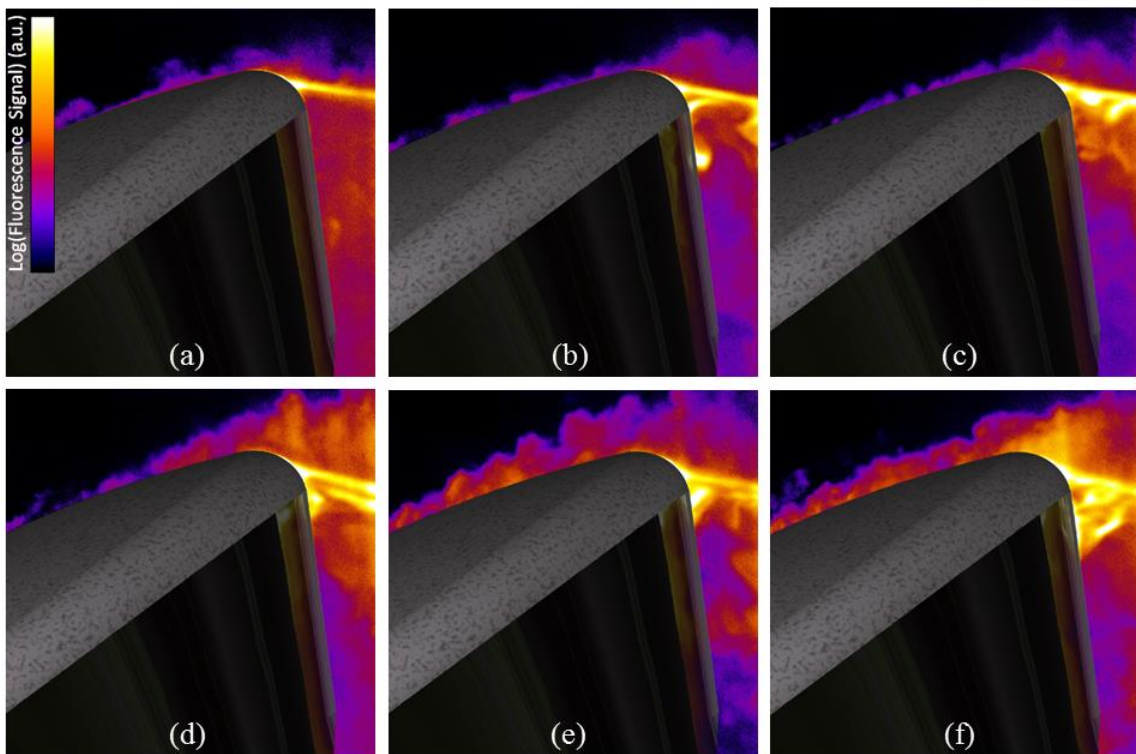


Fig. 12 Naphthalene PLIF images of a capsule model at 52° angle of attack focused on the capsule leeward shoulder. Images were collected during one run and images a-f are sequential in time, separated by approximately three seconds each.

Figures 13 through 16 depict the capsule model at various angles of attack with instantaneous naphthalene PLIF images superimposed on instantaneous Schlieren images. The naphthalene PLIF and Schlieren images

were not collected simultaneously. For the Schlieren imaging campaign, an aluminum heat shield was used. Therefore, the Schlieren images show no effects of ablation. In each figure a bow shock can be seen in front of the model and the standoff distance of the bow shock appears to decrease with increasing angle of attack. Expansion fans are also visible off both shoulders. Less obvious—and seen most clearly in Fig. 13(a)—are the shear layer and lip shock just downstream of the capsule shoulders. Shocks occurring as a result of the presence of the sting are seen in Figures 14 through 16. Also, a third expansion fan is visualized in Fig. 16 emanating from the aft edge of the windward capsule afterbody. These visualizations provide a way to view the naphthalene PLIF images in the context of the main features of the flowfield. One comparison that can be made between the Schlieren images and the naphthalene PLIF images is the location of the shear layer, which compares favorably in the figures below. The PLIF images show detailed information about the state of the boundary layer and shear layer that is not seen clearly in the Schlieren images. Furthermore, since the PLIF technique makes measurements on a planar slice whereas Schlieren images are path averaged, local flow information can be identified. For example, the Schlieren images (particularly Fig. 13(a) and Fig. 14(a)) appear to show a structure emanating from the middle of the capsule backshell. Combining the Schlieren and PLIF images, it can be determined that this is almost certainly a three-dimensional effect due to the path-integrated nature of the Schlieren technique. The structure is most likely the reflection of the bow shock off of the windows of the wind tunnel because if this flow feature was on the center plane of the capsule model there would be evidence of its existence in the naphthalene PLIF images shown in Fig. 13(b) and Fig. 14(b). Also, the flow in the capsule recirculation region is most likely not supersonic, so it is unlikely that a shock structure could be supported there. It would be difficult to draw such a definitive conclusion with the Schlieren imaging alone. However, the PLIF images do not visualize the flow features away from the model (i.e. shocks and expansion fans), hence the complimentary nature of the two techniques.

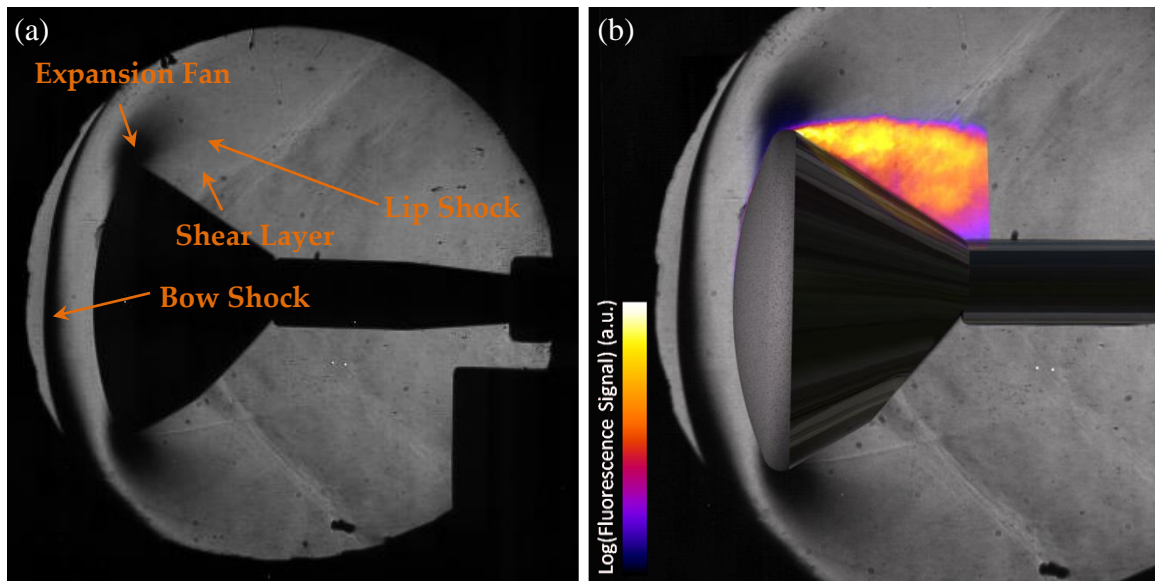


Fig. 13 Orion capsule model in a Mach 5 flow at 0° angle of attack with (a) Schlieren visualization and (b) naphthalene PLIF image superimposed on a Schlieren visualization of the flowfield.

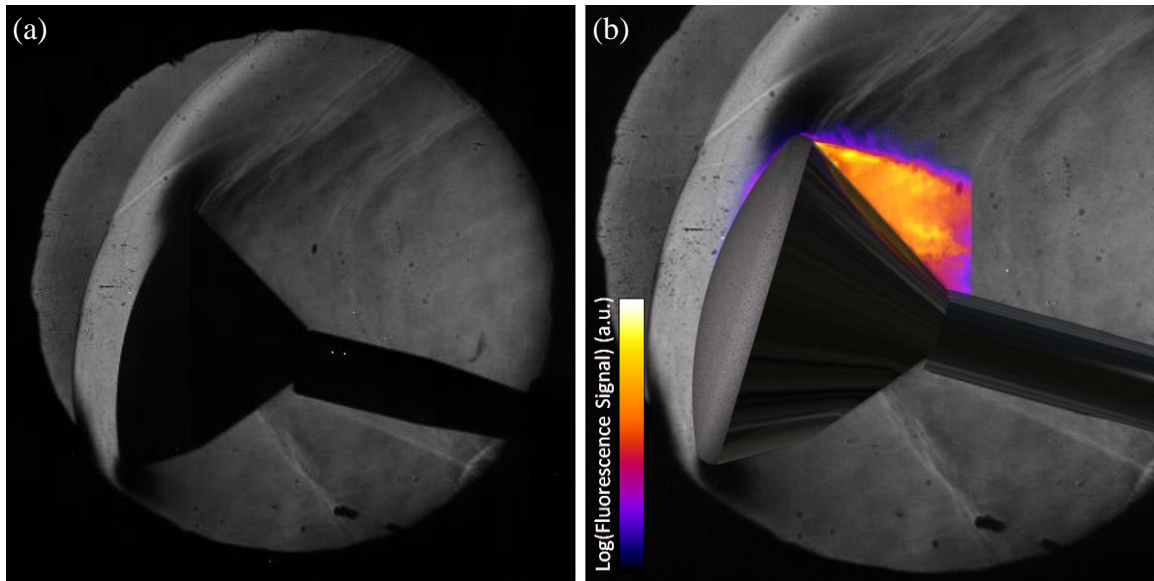


Fig. 14 Orion capsule model in a Mach 5 flow at 12° angle of attack with (a) Schlieren visualization and (b) naphthalene PLIF image superimposed on a Schlieren visualization of the flowfield.

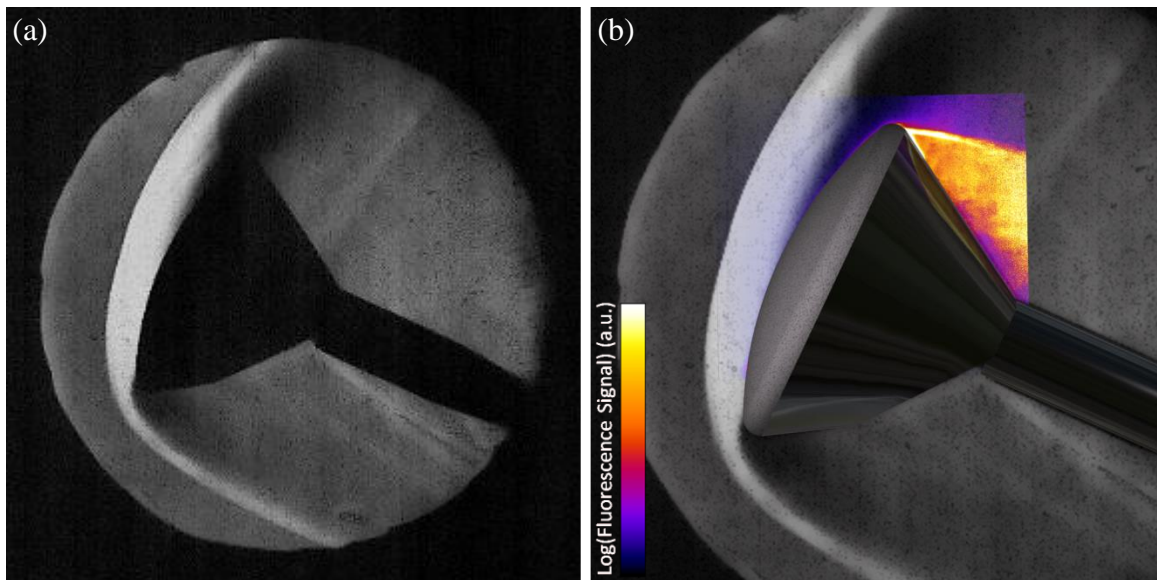


Fig. 15 Orion capsule model in a Mach 5 flow at 24° angle of attack with (a) Schlieren visualization and (b) naphthalene PLIF image superimposed on a Schlieren visualization of the flowfield.

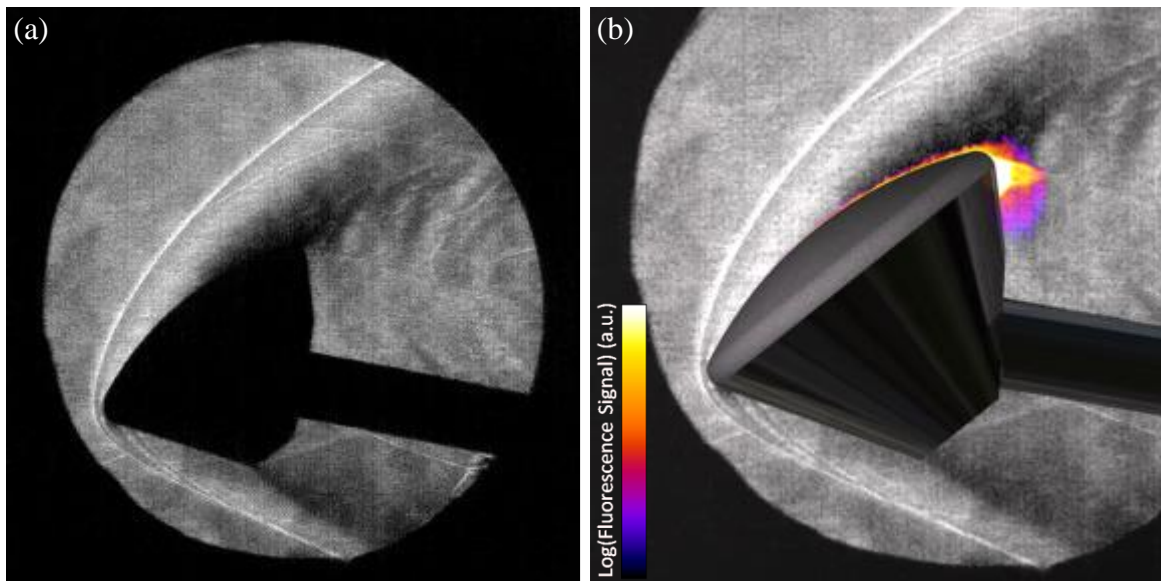


Fig. 16 Orion capsule model in a Mach 5 flow at 52° angle of attack with (a) Schlieren visualization and (b) naphthalene PLIF image superimposed on a Schlieren visualization of the flowfield.

4. Conclusion

Visualization of the dispersion of gas-phase ablation products on a scaled Orion MPCV model was performed using the naphthalene PLIF technique at four different angles of attack in a Mach 5 wind tunnel. It has been demonstrated that naphthalene PLIF is a promising technique for imaging ablation-products transport on a reentry capsule model. Schlieren imaging was used to complement the naphthalene PLIF flow visualization and the structure of the capsule shear layer compared favorably when imaged with both techniques. High concentrations of scalar were imaged in the capsule recirculation region using PLIF imaging and intermittent turbulent structures were visualized on the heat shield surface for the 12° and 52° angle of attack cases. The most prominent structures seen on the heat shield occurred for the 52° case, which consistently led to the visualization of the largest turbulent naphthalene structures on the heat shield surface. The shear layer appeared to be laminar for the 24° case, whereas for the 12° and 0° cases the shear layer appeared to transition from laminar to turbulent (or at least became more unsteady) over the course of the run. Not enough naphthalene vapor was visualized in the shear layer for the 52° case to make a determination as to the nature of the shear layer due to the positioning of the model in the camera's field of view. The shear layer appeared to be more turbulent at lower angles of attack and increasingly turbulent over the course of a wind tunnel run. The increased unsteadiness with run duration was most likely due to increased surface deformation and roughness, and possibly the increased blowing rate. It was also demonstrated using naphthalene PLIF imaging that the model would heat up over the course of a wind tunnel run, leading to more ablation and significantly more naphthalene present in the afterbody separated flow region. Other interesting flow features were identified in the PLIF images as well. First, the shear layer appeared to be approximately laminar at the leeward capsule shoulder compared to further downstream, which was consistent with previous research. Also, regions of relatively low naphthalene signal were identified in the capsule recirculation region. The low-signal regions consistently appeared in two distinct locations: just downstream of the leeward shoulder of the capsule and at the junction of the capsule model with the sting. These relatively steady flow features are most likely the result of spanwise structures, such as vortices, on the capsule afterbody. Additionally, a series of elongated naphthalene structures emanating from the upper edge of the shear layer were identified in multiple images collected at 12° angle of attack but the cause of this flow feature is currently undetermined.

Acknowledgements

This work was supported by a NASA Office of the Chief Technologist's Space Technology Research Fellowship Grant (#NNX11AN55H).

References

Alderfer, D. W., P. M. Danehy, J. A. Wilkes Inman, K. T. Berger, G. M. Buck, and R. J. Schwartz (2007) Fluorescence Visualization of Hypersonic Flow Over Rapid Prototype Wind-Tunnel Models. AIAA Paper 2007-1063, 45th AIAA Aerospace Sciences Meeting and Exhibit, Reno, Nevada.

Autodesk 3ds Max Product Information (2014), Autodesk Inc.

Buck, G. M., A. N. Watkins, P. M. Danehy, J. A. Inman, D. W. Aldefer, and A. A. Dyakonov (2008) Experimental Measurement of RCS Jet Interaction Effects on a Capsule Entry Vehicle. AIAA Paper 2008-1229, 46th AIAA Aerospace Sciences Meeting and Exhibit, Reno, Nevada.

Callaway, D. W., M. F. Reeder, R. B. Greendyke, and R. Gosse (2010) Photogrammetric Measurement of Recession Rates of Low Temperature Ablators in Supersonic Flow. AIAA Paper 2010-1216, 48th AIAA Aerospace Sciences Meeting, Orlando, Florida.

Charwat, A. F. (1968) Exploratory studies on the sublimation of slender camphor and naphthalene models in a supersonic wind-tunnel.

Combs, C. S., N. T. Clemens, P. M. Danehy, B. Bathel, R. Parker, T. Wadhams, M. Holden, and B. Kirk (2013) NO PLIF Visualizations of the Orion Capsule in LENS-I. AIAA Paper 2013-0033 51st AIAA Aerospace Sciences Meeting and Exhibit, Grapevine, Texas, Jan. 7-10.

Combs, C. S., N. T. Clemens, and P. M. Danehy (2014) Development of Naphthalene PLIF for Visualizing Ablation Products from a Space Capsule Heat Shield. AIAA Paper 2014-1152 52nd AIAA Aerospace Sciences Meeting and Exhibit, National Harbor, Maryland, Jan. 13-17.

Danehy, P. M., J. A. Wilkes, D. W. Alderfer, S. B. Jones, A. W. Robbins, D. P. Patry and R. J. Schwartz (2006) Planar laser-induced fluorescence (PLIF) investigation of hypersonic flowfields in a Mach 10 wind tunnel. AIAA Paper 2006-3442, AIAA AMT-GT Technology Conference, San Francisco.

Danehy, P. M., D. W. Alderfer, J. A. Inman, K. T. Berger, G. M. Buck, and R. J. Schwartz (2008) Fluorescence Imaging and Streamline Visualization of Hypersonic Flow Over Rapid Prototype Wind-Tunnel Models. Proceedings of the Institution of Mechanical Engineers, Part G: Journal of Aerospace Engineering, Vol. 222, No. 5, pp. 637-651.

Danehy, P. M., J. A. Inman, G. J. Brauckmann, D. W. Alderfer, S. B. Jones, and D. P. Patry (2009) Visualization of a Capsule Entry Vehicle Reaction-Control System (RCS) Thruster," Journal of Spacecraft and Rockets, Vol. 46, No. 1, pp. 93-102.

Du, H., R. A. Fuh, J. Li, A. Corkan, and J. S. Lindsey (1998) PhotochemCAD: A computer-aided design and research tool in photochemistry. Photochemistry and Photobiology, Vol. 68, pp. 141-142.

Gamba, M., M. G. Mungal, R. K. Hanson (2012) OH PLIF Imaging of the Reaction Zone in Combusting Transverse Jets in Supersonic Crossflow. 16th Int'l Symp. on Applications of Laser Techniques to Fluid Mechanics, Lisbon, Portugal.

Hanson, R. K., J. M. Seitzman, and P. H. Paul (1990) Planar Laser-Fluorescence Imaging of Combustion Gases. Applied Physics B, Vol. 50, pp. 441-454.

Ho, D. W. K., J. H. Koo, M. C. Bruns, and O. A. Ezekoye (2007) A Review of Numerical and Experimental Characterization of Thermal Protection Materials – Part III. Experimental Testing. AIAA 2007-5773, 43rd AIAA/ASME/SAE/ASEE Joint Propulsion Conference & Exhibit, Cincinnati, Ohio.

- Inman, J. A., P. M. Danehy, D. W. Alderfer, and G. M. Buck, A. McCrea, and R. J. Schwartz (2008) PLIF Imaging of Capsule RCS Jets and Simulated Forebody Ablation. AIAA Paper 2008-0248, 46th AIAA Aerospace Sciences Meeting and Exhibit, Reno, Nevada.
- Kaiser, S. A. and M. B. Long (2005) Quantitative planar laser-induced fluorescence of naphthalene as fuel tracers. Proceedings of the Combustion Institute, Vol. 30, pp. 1555-1563.
- Kohlman, D. L. and R. W. Richardson (1969) Experiments on the use of dry ice ablating wind-tunnel models. Journal of Spacecraft and Rockets, Vol. 6, No. 9, pp. 1061-1063.
- Kruif, C. G. de, T. Kuipers, J. C. van Miltenburg, R. C. F. Schaake, and G. Stevens (1981) The vapour pressure of solid and liquid naphthalene. Journal of Chemical Thermodynamics, Vol. 13, No. 11, pp. 1081-1086.
- Lipfert, F. and J. Genovese (1971) An experimental study of the boundary layers on low-temperature subliming ablaters. AIAA Journal, Vol. 9, No. 7, pp. 1330-1337.
- Lochman, B. (2010) Technique for Imaging Ablation-Products Transported in High-Speed Boundary Layers by using Naphthalene Planar Laser-Induced Fluorescence. Master's Thesis, University of Texas at Austin.
- Lozano, A., B. Yip, and R. K. Hanson (1992) Acetone: a tracer for concentration measurements in gaseous flows by planar laser-induced fluorescence. Experiments in Fluids, Vol. 13, pp. 369-376.
- Schwartz, R. J. (2003) ViDI: Virtual Diagnostics Interface Volume 1-The Future of Wind Tunnel Testing. Contractor Report NASA/CR-2003-212667.
- Silton, S. I. and D. B. Goldstein (2000) Ablation Onset in Unsteady Hypersonic Flow About Nose Tip with Cavity. Journal of Thermophysics and Heat Transfer, Vol. 14, No. 3, pp. 421-434.
- Smits, A. J., M. P. Martin, and S. Girimaji (2009) Current status of basic research in hypersonic turbulence. AIAA 2009-151, 47th AIAA Aerospace Sciences Meeting and Exhibit, Orlando, Florida.
- Stock, H. W. and J. J. Ginoux (1971) Experimental Results on Crosshatched Ablation Patterns. AIAA Journal, Vol. 9, No. 5, pp. 971-973.